RNA adenosine deaminase ADAR2 modulates T helper 17 cell effector function

Shengyun Ma[1,4], Benjamin S. Cho[1,4], Yuxin Li[1], Nazia Abbasi[1], Brian A. Yee[1], Ge Sun[1], Claire Luo[1], John T. Chang[2], Bing Zhou[1,3], Xiang-dong Fu[1], Gene W. Yeo[1], Wendy Jia Men Huang[1,*]

[1] Department of Cellular and Molecular Medicine,

University of California San Diego, La Jolla, CA 92093, U.S.A

[2] Department of Medicine,

University of California San Diego, La Jolla, CA 92093, U.S.A

[3] currently at Institute of Zoology Chinese Academy of Sciences, Beijing 100101, China

[4] These authors contributed equally.

* Correspondence: wendyjmhuang@health.ucsd.edu

SUMMARY

Adenosine deaminases acting on RNA (ADARs) catalyze the most common RNA modification in mammals, but it remains to be elucidated how their RNA editing dependent and independent activities contribute to host immunity. Here, we report dynamic changes in ADARs expressions and global adenosine-to-inosin (A-to-I) editome during T helper cell differentiation. In differentiated T helper 17 (Th17) cells, transcription of the ADAR2 encoding locus is potentiated by an intragenic super enhancer and splicing of the ADAR2 encoding transcript is further facilitated by a DEAD-box RNA helicase, DDX5. In an editing-independent manner, ADAR2 negatively regulates Hypoxia-Inducible Factor 1-alpha (HIF1α) expression to limit the production of interleukin-10 (IL-10) in Th17 cells. These results demonstrate ADAR2 and the upstream mechanisms governing its expression as critical regulators of Th17 cell effector function.

INTRODUCTION

Circulating naive $CD4^+$ T lymphocytes encountering their cognate antigens differentiate into cytokine-producing effector cells to coordinate local and systemic immune responses (Reiner, 2009). The interleukin-17 (IL-17) producing effector cells are known as T-helper 17 (Th17). Th17 cells are heterogenous and can be functionally subdivided into two groups. The homeostatic subsets of Th17 cells secrete IL-10 and suppress inflammation in healthy hosts (Aschenbrenner et al., 2018; Bellemore et al., 2015; Chaudhry et al., 2011; Esplugues et al., 2011; McGeachy et al., 2007; Tanaka et al., 2018; Wu et al., 2018). In contrast, pathogenic subsets of Th17 cells contribute to autoimmune diseases and secrete a combination of proinflammatory cytokines, including IL-17, IL-21, and Granulocyte-macrophage colony-stimulating factor (GM-CSF) (Codarri et al., 2011; Stockinger and Omenetti, 2017; Tigno-Aranjuez et al., 2009). Paradoxically, while antibody blockades of Th17 cytokines benefit patients with psoriasis and arthritis (Yasuda et al., 2019), they worsen disease outcomes in patients with inflammatory bowel disease (Hueber et al., 2012). Better understanding of the molecular mechanisms underlying Th17 cytokine heterogeneity may provide improved therapeutic strategies to maintain homeostatic Th17 functions and also selectively block Th17 pathogenicity.

Adenosine deaminase acting on RNA (ADAR) is a highly conserved protein family that catalyzes the deamination of adenosine to inosine (A-to-I editing), the most abundant RNA modification in the mammalian transcriptome (Gallo et al., 2017; Tan et al., 2017) The ADAR family includes two active proteins, ADAR1 (encoded by *Adar*) and ADAR2 (encoded by *Adarb1*), as well as one catalytically inactive member, ADAR3 (encoded by

Adarb2). ADAR1 and ADAR2 have shared and unique targets. They are unable to compensate for each other's essential functions *in vivo* (Chalk et al., 2019). ADAR1 primarily edits repetitive elements and prevents aberrant innate immune sensing of endogenous RNAs (Athanasiadis et al., 2004). ADAR2-mediated editing-dependent protein recoding of GRIA2 in neurons is essential for life (Higuchi et al., 2000). Importantly, ADARs also regulate other aspects of RNA biology independent of their catalytic activities. By binding to their target RNAs and interacting with other protein complexes, ADARs modulate alternative splicing, mRNA stability, microRNA biogenesis, and protein translation (Qi et al., 2017; Walkley and Li, 2017). In the immune system, ADAR1 in the thymus contribute to T cell maturation and self-tolerance (Nakahama et al., 2018). However, nothing is known about the editing dependent and independent roles of ADARs in mature T cells, including Th17.

Here, we report that naive and differentiated $CD4^+$ T lymphocytes harbored unique and overlapping A-to-I editomes. Induction of ADAR2 in Th17 is driven transcriptionally by an intragenic super enhancer and post-transcriptionally by an RNA binding protein DDX5. Surprisingly, ADAR2 modulates effector cytokine production in Th17 cells in an editing independent manner. By blocking the pre-mRNA processing of *Hif1a*, ADAR2 impaired the expression of HIF1α and its downstream target IL-10. Altered expression of ADAR2 or DDX5 in T cells result in dysregulated $HIF1\alpha^+IL\text{-}10^+$ Th17 population in the intestine.

RESULTS

Transcription regulation of *Adarb1* in Th17 cells

Total RNA-seq revealed that genes encoding different ADARs were dynamically expressed in $CD4^+$ naive and differentiated Th17 cells. In particular, while *Adar* transcripts, encoding ADAR1, were downregulated in Th17 cells, *Adarb1* transcripts, encoding ADAR2, were significantly upregulated (Figure 1A and 1B). Our observation is consistent with results from an independent RNA profile dataset (Figure S1A) (Stubbington et al., 2015). Western blot analyses confirmed that ADAR2 was abundantly expressed in Th17 cells (Figure 1C) and predominantly localized to the nucleus (Figure S2A).

Next, we sought to identify the *cis*-regulatory element(s) (CNS) and transcription factor(s) responsible for *Adarb1* transcriptional activation during naive to Th17 polarization. Genome-wide characterization of acetylation on lysine 27 of histone H3 (H3K27ac) revealed a putative intragenic super-enhancer at the *Adarb1* locus in Th17 cells (Figure 1D), containing four regions that opened up during naive to Th17 polarization (CNS1: chr10 77406713-77406733, CNS2: chr10 77388804-77388824, CNS3: chr10 77387874-77387894, and CNS4: chr10 77368829-77368848) and one genomic region that was shut down in Th17 cells (CNS5: chr10 77367402-77367422) (Figure 1E). Time-course chromatin accessibility assay (ATAC-seq) revealed that chromatin openings at the CNS2, CNS3, and CNS4 regions closely correlate with the accessibility of *Adarb1* promoter (Figure S3A), suggesting these CNSs may cooperate to drive *Adarb1* transcription. To test this possibility, small guide RNAs (sgRNAs) designed to target each of the putative

elements were introduced to Cas9-expressing Th17 cells. Targeting of the CNS2 and CNS3 regions resulted in significant reduction of *Adarb1* mRNA expression (Figure 1F).

Analysis of a published transcription factor chromatin-immunoprecipitation (ChIP-seq) dataset (Ciofani et al., 2012) identified three Th17 master transcription factors, Basic Leucine Zipper ATF-Like Transcription Factor (BATF), Interferon Regulatory Factor 4 (IRF4), and RAR-related Orphan Receptor gamma (RORγt), were recruited to the *Adarb1* super enhancer region in Th17 cells (Figure 1G). Analysis of a published transcriptomic dataset of Th17 cells obtained from BATF, IRF4, or RORγt knockout mice (Ciofani et al., 2012) revealed that *Adarb1* expression was IRF4 dependent, and BATF and RORγt independent (Figure 1H). In summary, *Adarb1* transcription in Th17 cells is facilitated by regional chromatin reorganization coupled to the establishment of an IRF4 occupying intragenic super enhancer.

Naive and polarized Th17 cells have overlapping and distinct A-to-I RNA editomes

ADARs catalyze RNA adenosine deamination. We hypothesized that the dynamic expression patterns of ADARs in naive and polarized Th17 cells would orchestrate distinct A-to-I editomes in these cells. To test this possibility, A-to-I edited transcripts from two independent biological replicates of naive and Th17 cells were identified using the Software for Accurately Identifying Locations of RNA-editing (SAILOR) (Washburn et al., 2014). With confidence scores greater than 0.99, we found 571 and 399 A-to-I edited sites, corresponding to transcripts from 270 and 131 genes, in naive and Th17 cells respectively (Figure 2A and Table S1). Majority of the edited sites localized to 3'

untranslated regions (UTRs) (Figure 2B), similar to previous reports in other cell types (Athanasiadis et al., 2004; Qiu et al., 2016). Edited transcripts in naive and Th17 conditions had less than 18% overlap and encode for molecules enriched in different pathways, including T cell receptor signaling in naive cells and cytokine production in Th17 cells (Figure 2C and 2D).

ADAR2 targets *Hif1a* transcripts to regulate Th17 effector cytokine production

Several Th17 transcripts with A-to-I edits encode critical regulators of Th17 effector functions, including the Hypoxia-inducible factor alpha (HIF1α), C-C Chemokine Receptor 4 (CCR4), Interleukin-21 (IL-21), and Zinc finger and BTB domain containing 7B (ZBTB7B, also known as ThPok) (Figure 2E). Unlike most transcripts with A-to-I edits at the 3' UTR, the *Hif1a* transcript was edited at its 12th intron. Immunoprecipitation using the anti-ADAR2 specific antibody suggested that ADAR2 associated with both the pre-processed and mature *Hif1a* transcript in Th17 cells (Figure S4A). Overexpression of wild type ADAR2, but not the enzymatically dead version (ADAR2^{E396A}), enhanced the fraction of *Hif1a* transcripts harboring adenosine deamination (Figure 3A and 3B). These results demonstrate that ADAR2 binds to and edits *Hif1a* transcripts in Th17 cells.

Next, we asked whether ADAR2 targets *Hif1a* transcript to regulate HIF1α expression. Intracellular protein staining revealed that cells overexpressing wild type ADAR2 had reduced HIF1α levels compared to control cells (Figure 3C and 3D). Surprisingly, overexpression of the enzymatically dead ADAR2 also dampened HIF1α protein levels. In ADAR2^{E396A}-expressing Th17 cells, significant accumulation of unspliced *Hif1a* pre-

mRNA was observed (Figure 3E and S5A). In contrast, CRISPR-Cas9 mediated knock down of ADAR2 lowered the fraction of *Hif1a* transcripts being edited and potentiated their proper splicing in Th17 cells (Figure 3F, 3G and 3H). These results highlight unexpected roles of ADAR2 in regulating *Hif1a* transcripts and protein expression through both enzymatic activity dependent and independent mechanisms.

HIF1α is a major regulator of cytokine IL-10 expression in B cells (Meng et al., 2018). Similarly, CRISPR-Cas9 mediated knock down of HIF1α also reduced IL-10 expression in Th17 cells (Figure 4A, 4B and 4C). Therefore, we hypothesized that negative regulation of HIF1α expression by ADAR2 would affect IL-10 production in Th17 cells (modeled in Figure 4D). Indeed, overexpression of either wild type or mutant ADAR2 was sufficient to dampen IL-10 production in cultured Th17 cells (Figure 4E and 4F). To assess the role of ADAR2 in $CD4^+$ T cells *in vivo*, activated $CD4^+$ T cells transduced with $ADAR2^{WT}$ or $ADAR2^{E396A}$ overexpression constructs were transferred into RAG1 knockout mice. Compared to empty vector transduced controls, recipients of either $ADAR2^{WT}$ or $ADAR2^{E396A}$ overexpressed cells experienced greater weight loss (Figure 4G), and $ROR\gamma t^+$ Th17 cells recovered from their small intestine had reduced HIF1α and IL-10 expression (Figure 4H, 4I, and 4J). Interestingly, changes in ADAR2 expression did not significantly modulate HIF1α and IL-10 levels in the colon, suggesting ADAR2 likely regulates Th17 cell effector function in a tissue specific manner. In summary, these results demonstrate that ADAR2 negatively regulates HIF1α and IL-10 expression in Th17 cells *in vitro* and *in vivo*.

***Adarb1* pre-mRNA processing is regulated by DDX5 in Th17 cells**

Previous studies suggest that transcripts encoding proteins involved in RNA metabolism, such as *Adarb1*, are often regulated by other RNA binding proteins (RBP), including members of the DEAD-box (DDX) family of RNA helicases (Palladino et al., 2000). In Th17 cells, the most abundant transcript encoding DDXs is *Ddx5* (Figure S6A) (Stubbington et al., 2015). Enhanced cross-linked immunoprecipitation analysis (eCLIP-seq) using the DDX5-specific antibodies (Figure S6B) revealed several DDX5 footprints on the first intron of the *Adarb1* transcript (Figure 5A). DDX5 can associate with heterogeneous nuclear ribonucleoprotein (hnRNP) and U1 small nuclear ribonucleoproteins to facilitate pre-mRNA splicing (Lin et al., 2005; Liu, 2002). To test the possibility that perhaps DDX5 binds to *Adarb1* transcripts to regulate their post-transcriptional processing, wild type and DDX5-deficient Th17 cells were treated with flavopiridol, a transcription inhibitor, for eight hours and harvested to assess the ratio of spliced and unspliced *Adarb1* transcripts as described in Figure S5. Loss of DDX5 resulted in a significant increase in the ratio of unspliced over spliced *Adarb1* transcripts (Figure 5B). qRT-PCR and western blot analyses confirmed that DDX5 knocked out Th17 cells had lowered *Adarb1* mRNA and ADAR2 protein (Figure 5C and 5D). Notably, RNA-seq analyses of wild type and DDX5-deficient Th17 cells revealed that the expression of *Irf4*, encoding the transcription factor required for *Adarb1* induction in Th17, was not affected in DDX5 knocked out Th17 cells (Figure S7A).

Unlike *Adarb1*, *Adar* transcripts did not carry any DDX5 footprint and mature *Adar* mRNA was upregulated in DDX5-deficient Th17 cells, which perhaps to compensate for the loss

of *Adarb1* expression (Figure S7B). We hypothesize that the imbalance of ADAR1 and ADAR2 expression in DDX5 knocked out Th17 cells may result in a dysregulated A-to-I editome. Indeed, SAILOR analyses of the transcriptome from two independent pairs of wild types and DDX5-deficient Th17 cells (Figure S8A and Table S2) uncovered a subset of Th17 transcripts harboring DDX5-dependent A-to-I edits (Figure 5E and Table S2), including *Hif1a* and the transcript encoding Apolipoprotein B Editing Complex 3 (*Apobec3)* (Figure S8B). PCR and Sanger sequencing of independent biological replicates confirmed significantly reduced fraction of these transcripts harboring A-to-I edits in DDX5-deficient Th17 cells (Figure 6A and S8C).

In the absence of DDX5, reduced ADAR2 levels and *Hif1a* editing were accompanied with an elevated expression of HIF1α and IL-10 (Figure 6B and 6C). CRISPR-Cas9 mediated mutation of a DDX5 bound region of *Adarb1* promoted similar increases in HIF1α and IL-10 (Figure 6D and 6E). *In vivo*, aberrant HIF1α $^{+}$IL-10^{+} expressing Th17 cells were found in the small intestine from DDX5 T-cell specific knockout of mice (Figure 6F). In summary, these results demonstrate that DDX5 regulates ADAR2 expression to fine-tune Th17 editome and effector cytokine production (modeled in Figure 6G).

DISCUSSION

ADARs not only catalyze RNA deamination, the most common RNA modification in mammals, they also had a number of catalytic activity-independent functions. For example, binding of ADAR1 to the *Ctn* RNA, independent of A-to-I editing, is sufficient to promote *Ctn* RNA stability by limiting the access of RNA decay complexes

(Anantharaman et al., 2017). However, little is known about the molecular mechanisms governing ADAR expressions and their A-to-I editing dependent as well as independent functions in immune system. Identification and characterization of A-to-I edited transcripts in naive and Th17 cells uncovered the *Hif1a* transcript as a unique target of ADAR2 in Th17 cells. Unlike majority of A-to-I edited sites localizing to the 3'UTR, *Hif1a* is edited on intron 12 by ADAR2. Surprisingly, ADAR2 also negatively regulates *Hif1a* pre-mRNA processing in an enzymatic activity independent manner. We speculate that both passive and active mechanisms could be involved in this regulation. For instance, ADAR2 binding to *Hif1a* splicing junctions could directly limit the accessibility of the RNA transcript to the splicing machinery. ADAR2 may also recruit and/or cooperate with other negative regulators of splicing to form large protein complexes to interfere with *Hif1a* processing indirectly (Tang et al., 2020). Future studies will be needed to evaluate these possibilities.

HIF1α is a hypoxia inducible factor and plays important roles fine-tuning Th17 effector function in response to local tissue environment (Dang et al., 2011). Hypoxia has been known to promote IL-10 expression (Volchenkov et al., 2017). In $CD1d^{hi}CD5^{+}$ B cells, HIF1α promotes IL-10 expression to protect against autoimmunity (Meng et al., 2018). Similarly, here we report that HIF1α also promotes IL-10 expression in Th17 cells. Importantly, this pathway is regulated by ADAR2. Loss of ADAR2 expression results in an increase of HIF1α and IL-10 levels in Th17 cells of the intestine.

ADARs expressions in naive and differentiated T cells are dynamically regulated. In Th17 cells, ADAR2 is induced in an IRF4 and intragenic super enhancer dependent manner.

And processing of the *Adarb1* pre-mRNAs is facilitated by an RNA-binding protein of the DEAD-box family, DDX5. Alterations in ADAR2 or DDX5 levels disrupt global A-to-I editing in Th17 cells and perturb the ability of homeostatic Th17 cell to make IL-10 cytokines in the small intestine. Intriguingly, colonic Th17 cells are not governed by the ADAR2-DDX5 axis. We speculate that this regional specificity is likely due to a combination of unique signaling molecules present in each microenvironment and the distinct repertoires of transcription factor expressed in Th17 cells from different tissues. Future studies will be needed to test whether increase of intestinal HIF1α $^{+}$IL-10^{+} Th17 cells in the T cell specific DDX5 knockout mice would alter host sensitivity to local inflammatory challenges, whether other DDX family members homologous to DDX5, such as DDX17, can compensate for the loss of DDX5 activities in disease settings, as well as whether the DDX5-ADAR2 mechanism described here can also contribute to regulating HIF1α-IL-10 expression in other cells types and in other tissue environments. Uncovering the roles of ADARs and A-to-I editing in T cells provide better understanding of the mechanisms regulating homeostatic Th17 effector functions and reveal new therapeutic targets for modulating their activities in health and disease.

ACKNOWLEDGEMENTS

We thank Frances Fuller-Pace at the University of Dundee for sharing the DDX5 conditional mutant mice previously described in (Nicol et al., 2013). We thank Stefan Aigner, Alan Domissy, and Thai Bao Nguyen from the Gene Yeo Laboratory at the University of California San Diego for advice and technical support on the eCLIP-seq assays. We thank Johannes Zuber and Aichinger Martin at the Research Institute of Molecular Pathology (I.M.P.) for sharing the pSIN vector for generating retroviruses to carry custom sgRNAs into T cells. We thank Karen Sykes for suggestions to the manuscript. We thank Elina Zuniga and Li-Fan Lu for critiques and feedback to the project as members of the Master's thesis committee for B.S.C.

S.M., B.S.C., N.A., C.L. and W.J.M.H. are partially funded by the Edward Mallinckrodt, Jr. Foundation and the National Institutes of Health (NIH) (R01 GM124494 to WJM Huang). B.A.Y. and G.W.Y. are partially funded by NIH (R01 HG004659 and U41 HG009889 to GW Yeo). J.T.C. is partially funded by NIH (R01 AI129973). Illumina sequencing was conducted at the IGM Genomics Center, University of California San Diego, with support NIH (S10 OD026929) and Moores Cancer Center (P30 CA023100).

AUTHOR CONTRIBUTIONS

S.M. designed and performed ChIP-seq, ATAC-seq, RNA-seq, and flow cytometry studies. B.S.C. completed the *Hif1a* editing and *Adarb1* splicing studies in Th17 cells with help from S.G. Y.L. performed the RNA-seq analyses (DESeq2, SAILOR, and Gene Ontology). N.A. designed and performed the eCLIP-seq experiment in Th17 cells. B.A.Y.

performed bioinformatics analyses on the eCLIP-seq datasets. C.L. designed and performed sgRNA studies to assess enhancer activities of the *Adarb1* regulatory elements. J.T.C. contributed resources and edited the manuscript. B.Z. performed the enhancer and super enhancer analyses on the ChIP-seq datasets. X.D.F. directed the enhancer analyses by B.Z. and edited the manuscript. G.W.Y directed analyses on the eCLIP-seq datasets and SAILOR and edited the manuscript. W.J.M.H. analyzed and wrote the manuscript together with S.M and B.C.

DECLARATION OF INTERESTS

GW Yeo is co-founder, member of the Board of Directors, on the Science Advisory Board, equity holder, and paid consultant for Locanabio and Eclipse BioInnovations. GW Yeo is a visiting professor at the National University of Singapore. GW Yeo's interests have been reviewed and approved by the University of California San Diego in accordance with its conflict of interest policies. All other authors declare no competing financial interests.

FIGURE TITLES AND LEGENDS

Figure 1. **An intragenic super enhancer promotes *Adarb1* transcription in Th17 cells**

A. Volcano plot of RNA-seq results from $CD4^+$ naive (n=2) and cultured Th17 cells (n=2). Black dots: differentially expressed genes defined as $\log_2$ fold change ≥ 1 and *p*-value <0.05.

B. Heatmap of RNA expressions as determined by DEseq2 analysis of the RNA-seq dataset from A. Results from two independent biological replicates are shown.

C. Representative western blot analysis of whole cell extracts from $CD4^+$ naive and Th17 cells. ADAR2 expression is quantified as signal of anti-ADAR2 antibody over those from the total protein stain. This experiment was repeated three times on independent biological samples with similar results.

D. Normalized histone H3 lysine 27 acetylation signals (RPM) in genomic regions within a 12.5 Kb window outside of any known-gene promoters (TSS ± 2.5 Kb). Regions above the geometrically defined inflection point from this representation were considered putative super-enhancers (SE) and those below were consider putative traditional enhancers (TE) similar to previous report (Loven et al., 2013).

E. Integrative Genomic Viewer (IGV) displayed of the putative *Adarb1* super enhancer identified in D. Chromatin accessibility of the locus was assessed by two independent ATAC-seq time course experiments on $CD4^+$ naive T cells and Th17 cells harvested at 48 or 72 hours.

F. Log_2 fold changes in *Adarb1* mRNA quantified by qRT-PCR in $Cas9^+$ Th17 cells transduced with sgRNAs targeting the corresponding CNS compared to control.

Average and standard deviation from two biological replicates are shown. * *p*-value<0.05, ** *p*-value<0.01 (t-test).

G. IGV display of BATF, IRF4, p300, and RORγt occupancies as determined by ChIP-seq (GSE40918) (Ciofani et al., 2012) on the *Adarb1* super enhancer.

H. Expression of *Adarb1* in Th17 cell from WT, BATF, IRF4, and RORγt knockout mice as determined by RNA-seq (Ciofani et al., 2012). *** *p*-value<0.001.

Figure 2. **Overlapping and unique A-to-I editomes in wild type naive and Th17 cells**

A. Fraction of transcripts harboring A-to-I edits as defined by SAILOR analysis on the RNA-seq datasets. Each dot represents transcripts from one gene. Linear regression line was used to calculate correlation score (R^2) from two independent biological replicates of naive and Th17 cells.

B. Distribution of A-to-I edited sites on naive and Th17 transcripts from A.

C. The top 5 gene ontology pathways enriched in proteins encoded by A-to-I edited transcripts in naive and Th17 cells.

D. Shared and distinct A-to-I editomes in naive and Th17 cells.

E. RNA expression and % A-to-I editing of *Ccr4*, *Hif1a*, *Il21*, and *Zbtb7b* transcripts in naive and Th17 cells as determined by DEseq2 and SAILOR. Each dot represents result from one biological replicate (naive, n=2; Th17, n=2).

Figure 3. **ADAR2 negatively regulates HIF1α expression in Th17 cells**

A. Representative western blot analysis of whole cell extracts from Th17 cells transduced with empty, $ADAR2^{WT}$, or enzymatically dead $ADAR2^{E396A}$ expression

constructs. This experiment was repeated two times on independent biological samples with similar results.

B. Representative RT-PCR and Sanger sequencing analyses on *Hif1a* transcripts from control, $ADAR2^{WT}$, or enzymatically dead $ADAR2^{E396}$ overexpressed Th17 cells. Results are representative from two independent experiments.

C. Representative flow cytometry analysis of HIF1α and RORγt expression in Th17 cells transduced with control (black), $ADAR2^{WT}$ (red), or enzymatically dead $ADAR2^{E396}$ (blue) expression constructs.

D. Summarized flow cytometry analysis results from three independent experiments described in C. * *p*-value<0.05 (paired t-test).

E. Ratio of unspliced to spliced *Hif1a* transcripts in control and $ADAR2^{E396}$ expressing Th17 cells as assessed by qRT-PCR. Each dot represents result from one biological replicate (control, n=4; $ADAR2^{E396}$, n=4). * *p*-value<0.05 (paired t-test).

F. Representative western blot analysis of whole cell extracts from $Cas9^{+}$ Th17 cells transduced with retrovirus carrying empty or sgRNA expression constructs designed to target the ATG translation start codon of *Adarb1*. This experiment was repeated three times on independent biological samples with similar results.

G. Representative RT-PCR and Sanger sequencing analyses on *Hif1a* transcripts from Th17 cells described in F, showing reduced A-to-I editing of *Hif1a* in ADAR2 knocked down cells. Results are representative from two independent experiments.

H. Ratio of unspliced to spliced *Hif1a* transcripts in control and ADAR2 knocked down Th17 cells as determined by qRT-PCR. * *p*-value<0.05 (t-test, n=4).

Figure 4. **ADAR2-HIF1α regulates IL-10 production in Th17 cells *in vitro* and *in vivo***

A. Representative flow cytometry analysis of IL-10 and HIF1α expression in Cas9^{+} Th17 cells transduced with control or *Hif1a* targeting sgRNA expression constructs. This experiment was repeated four times on independent biological samples with similar results.

B. Geometric mean fluorescent intensity (GMI) of HIF1α and RORγt in cells from experiments described in A. * *p*-value<0.05 (paired t-test, n=4).

C. Percentage of HIF1α and/or IL-10 expressing in cells from experiments described in A. ** *p*-value<0.01 (paired t-test, n=4).

D. Working model: ADAR2 targets *Hif1a* transcripts to negatively regulate HIF1α and its downstream target gene expression in Th17 cells.

E. Representative flow cytometry analysis of IL-10 expression in Th17 cells transduced with control, ADAR2^{WT}, or enzymatically dead ADAR2^{E396} expression constructs. This experiment was repeated three times on independent biological samples with similar results.

F. Summarized flow cytometry analysis results from independent experiments described in E. * *p*-value<0.05 and ** *p*-value<0.01 (paired t-test, n=3).

G. Weight changes of Rag1 knockout mice receiving control (n=6), ADAR2^{WT} (n=4), or enzymatically dead ADAR2^{E396} (n=4) overexpressing CD4^{+} T cells. * *p*-value<0.05 and ** *p*-value<0.01 (Mann-Whitney test).

H. GMI of HIF1α in CD90.1^{+}CD4^{+} cells from the colonic and ileal lamina propria of the Rag1 knockout mice described in G on day 38. * *p*-value<0.05 (t-test).

I. Proportion of RORγt^{+}HIF1α^{+} T helper cells in colonic and ileal lamina propria harvested from recipient mice described in G on day 38. * *p*-value<0.05 (t-test).

J. Proportion of HIF1α^{+}IL-10^{+} T helper cells in colonic and ileum lamina propria harvested from recipient mice described in G on day 38. * *p*-value<0.05 (t-test).

Figure 5. ***Adarb1* is post-transcriptionally regulated by RNA binding protein DDX5**

A. Left: schematic representation of the DDX5 enhanced CLIP (eCLIP-seq) experiment. Right: IGV display of DDX5 eCLIP-seq signals on *Adarb1* in Th17 cells.

B. Ratio of unspliced over spliced *Adarb1* transcripts in WT^{T} and DDX5$^{\Delta T}$ Th17 cells treated with flavopiridol (10 μM) for eight hours from three independent biological replicates. * *p*-value<0.05 (t-test).

C. Relative expression of mature *Adarb1* mRNA as assessed by qRT-PCR from three independent biological replicates of WT^{T} and DDX5$^{\Delta T}$ Th17 cells. *Gapdh* was used for normalization. ** *p*-value<0.01 (t-test).

D. Representative western blot analysis of whole cell extracts from WT^{T} and DDX5$^{\Delta T}$ Th17 cells. This experiment was repeated three times on independent biological samples with similar results.

E. Transcripts with DDX5-dependent and independent A-to-I edits as defined by SAILOR analysis of two independent biological replicates of WT^{T} and DDX5$^{\Delta T}$ Th17 cells.

Figure 6. **DDX5 promotes HIF1α -IL-10 axis *in vitro* and *in vivo***

A. Representative RT-PCR Sanger sequencing analysis of *Hif1a* transcripts in WT^T and $DDX5^{\Delta T}$ Th17 cells. This experiment was repeated two times on independent biological samples with similar results.

B. Representative flow cytometry analysis of HIF1α and IL-10 expression in WT^T and $DDX5^{\Delta T}$ Th17 cells polarized under IL-6 (20 ng/ml) and various TGFβ concentrations (0-5.0 ng/ml). This experiment was repeated three times on independent biological samples with similar results.

C. Summarized flow cytometry analysis results from three independent experiments described in B. * *p*-value<0.05 (t-test).

D. Representative flow cytometry analysis of RORγt, HIF1α, and IL-10 expression in $Cas9^+$ Th17 cells transduced with empty or sgRNAs targeting DDX5 binding site (S3) on *Adarb1*. This experiment was repeated three times on independent biological samples with similar results.

E. Summarized flow cytometry analysis results from three independent experiments described in D. * *p*-value<0.05 (paired t-test).

F. HIF1α and IL-10 expression in $CD4^+$ T cells from the distal small intestine (ileum) of WT^T and $DDX5^{\Delta T}$ mice. * *p*-value<0.05 (paired t-test, n=5).

G. Working model: DDX5 and ADAR2 are negative regulators of the HIF1α-IL-10 axis in Th17 cells.

METHODS

Mice

C57BL/6 wild-type (Stock No: 000664), Cas9 (Stock No: 026179), *CD4Cre* (Stock No: 017336), and Rag1 KO (Stock No: 002216) were obtained from the Jackson Laboratory. *DDX5*^{flox} mice were obtained from Dr. Frances Fuller-Pace's laboratory and have been previously described (Nicol et al., 2012). Heterozygous mice were bred to yield 6-8 weeks old *Ddx5*$^{+/+}$*CD4Cre*$^{+}$ (subsequently referred to as wild type, WT^{T}) and *Ddx5*$^{fl/fl}$ *CD4Cre*$^{+}$ littermates (referred to as DDX5$^{\Delta T}$). Adult mice at least eight weeks old were used. All animal studies were approved and followed the Institutional Animal Care and Use Guidelines of the University of California San Diego.

Th17 Cell Culture

Mouse naive T cells were purified from spleens and lymph nodes of 8-12 weeks old mice using the Naive CD4^{+} T Cell Isolation Kit according to the manufacturer's instructions (Miltenyi Biotec). Cells were cultured in Iscove's Modified Dulbecco's Medium (IMDM, Sigma Aldrich) and supplemented with 10% heat-inactivated FBS (Peak Serum), 50 U penicillin-streptomycin (Life Technologies), 2 mM glutamine (Life Technologies), and 50 μM β-mercaptoethanol (Sigma Aldrich). For polarized Th17 cell polarization, naive cells were seeded in 24-well or 96-well plates pre-coated with rabbit anti-hamster IgG and cultured in the presence of 0.25 μg/mL anti-CD3ε (eBioscience), 1 μg/mL anti-CD28 (eBioscience), 0.1-5.0 ng/mL TGF-β (R&D Systems), and 20 ng/mL IL-6 (R&D Systems) for 48 to 72 hours.

Retrovirus Transduction in T cells

sgRNAs were designed by CHOPCHOP (Labun et al., 2019)and the expressing retroviral constructs were generated as described previously (Ran et al., 2013). sgRNA sequences are listed in Table S3. Mouse ADAR2 overexpression constructs was generated by the In-Fusion® HD Cloning Plus kit (Takara). Specifically, primers were designed using Takara Primer Design tool with NotI and SalI extensions. The *Adarb1* amplified PCR product was combined with the NotI and SalI linearized MSCV vector (RRID:Addgene_17442). ADAR2^{E396A} expression construct was generated using the Q5 Site-Directed Mutagenesis Kit (NEB). Clones were screened and sequenced. Primers sequences are listed in Table S4.

PlatE cells were used to generate retrovirus as described (Morita et al., 2000). Virus transduction in T cells were performed 24 hours after T cell activation by centrifugation at 2000 rpm for 90 min at 32 ^{o}C. Live and Thy1.1^{+} retrovirus transduced cells cultured in Th17 polarizing conditions were analyzed by flow cytometry at 72 hrs.

Flow Cytometry

Cells were stimulated with 5 ng/mL Phorbol 12-myristate 13-acetate (PMA, Millipore Sigma) and 500 ng/mL ionomycin (Millipore Sigma) in the presence of GolgiStop (BD Bioscience) for 5 hours at 37 ˚C, followed by cell surface marker staining for CD4 (clone GK1.5; Biolegend) and CD90.1/Thy1.1 (clone HIS51; eBioscience). Fixation/Permeabilization buffers (eBioscience) were used as per manufacturer

instructions to assess intracellular transcription factor and cytokine expression. Antibodies are listed in Table S5.

RNA-seq

Ribosome-depleted RNAs were used to prepare sequencing libraries. 100 bp paired-end sequencing was performed on an Illumina HiSeq4000 by the Institute of Genomic Medicine at the University of California San Diego. Each sample yielded approximately 30-40 million reads. Paired-end reads were aligned to the mouse mm10 genome with the STAR aligner version 2.6.1a (Dobin et al., 2013) using the parameters: "--outFilterMultimapNmax 20 --alignSJoverhangMin 8 --alignSJDBoverhangMin 1 --outFilterMismatchNmax 999 --outFilterMismatchNoverReadLmax 0.04 --alignIntronMin 20 --alignIntronMax 1000000 --alignMatesGapMax 1000000". Uniquely mapped reads overlapping with exons were counted using featureCounts (Liao et al., 2014) for each gene in the GENCODE.vM19 annotation. Differential expression analysis was performed using DESeq2 (v1.18.1 package) (Love et al., 2014), including a covariate in the design matrix to account for differences in harvest batch/time points. Regularized logarithm (rlog) transformation of the read counts of each gene was carried out using DESeq2. Pathway analysis was performed on differentially expressed protein coding genes with minimal counts of 10, $\log_2$ fold change cutoffs of ≥ 0.5 or ≤ -0.5, and p-values <0.05 using Gene Ontology (http://www.geneontology.org/) where all expressed genes in the specific cell type were set as background.

Transcripts harboring A-to-I edits in the RNA-seq datasets were identified by SAILOR version 1.0.4 in the paired-end mode (Washburn et al., 2014). Hits with confidence score less than 0.99 were filtered out. Known genomic variations were obtained from the Mouse Genomes Project. Variants were removed from the resulting candidate list if they overlapped with the known genomic variations. All remaining candidates were annotated based on GENCODE.vM19.

ChIP-seq and ATAC-seq

ChIP-seq were performed on 5-10 million Th17 cells crosslinked with 1% formaldehyde. Chromatin were sonicated and immunoprecipitated using antibodies listed on Table S5 and Dynabeads (ThermoFisher Scientific), followed by reverse cross-linking, and library construction as described in (Kaikkonen et al., 2013). ATAC-seq libraries were generated as described in (Buenrostro et al., 2015). ChIP-seq and ATAC-seq processing followed the ENCODE guideline with some modifications (Landt et al., 2012). Specifically, single-end raw reads were mapped to the mouse genome (GENCODE assembly GRCm38) by bowtie2 (Version 2.3.4.1) in the local mapping mode with parameter "--local", followed by PCR deduplication by SAMTools (Version 1.9) with the utility markedup (Li et al., 2009). Mapped reads from each sample repeats were merged into a single BAM file by SAMTools, and peaks were called using MACS2 (Version 2.2.6) (Zhang et al., 2008) in the narrow peak-calling mode with default parameters for ChIP-seq data or specific parameters of "callpeak --nomodel --extsize 100" for ATAC-seq data. Regions with peak-score below 30 were filtered out and the remaining reliable peak profiles were

transformed into bigwig format and visualized on the Integrative Genomics Viewer (IGV Version 2.8.2) (Thorvaldsdottir et al., 2013).

Identification of Enhancers and Super-enhancers

Accessible chromatin regions away from known promoters (TSS± 2.5kb) and overlapped with H3K27ac ChIP-seq peaks were defined as putative enhancers. Promoter-enhancer co-openness correlation score was calculated as previously described in (Zhou et al., 2019). To identify super-enhancers, H3K27ac peak regions within a 12.5 Kb window outside of any known-gene promoters (TSS ± 2.5 Kb) were stitched together and ranked by increasing total background subtracted ChIP-seq occupancy of H3K27ac. Ranked regions were plotted against the total background subtracted ChIP-seq occupancy of H3K27ac in units of total rpm on the y-axis. Regions above the geometrically defined inflection point from this representation were considered putative super-enhancers similar to previous report (Loven et al., 2013).

DDX5 eCLIP-seq and ADAR RIP

eCLIP-seq analysis was performed as previously described (Van Nostrand et al., 2016). Primary cultured Th17 from two 8-10 weeks old wild-type (C57BL/6) female mice were subjected to UV-mediated crosslinking, lysis, and treatment with RNases, followed by immunoprecipitation (IP) of the DDX5-containing RNA complexes. RNA fragments protected from RNase digestion were subjected to RNA linker ligation, reverse-transcription, and DNA linker ligation to generate eCLIP-seq libraries for high-throughput Illumina sequencing. Peaks were first defined using CLIPper on the IP sample

(https://github.com/YeoLab/clipper/wiki/CLIPper-Home). Enrichments were calculated using both the IP and input samples. Log_2 fold change was calculated as eCLIP-seq reads normalized for read depth over normalized reads found at each peak region in the size-matched input sample. Significance tests were performed using the Fisher's exact test or chi squared test, as described (Van Nostrand et al., 2016). ENCODE Irreproducible Discovery Rate (IDR) analysis was performed on two independent biological replicates of Th17 cells. Peaks were ranked using the entropy formula, $Pi*log(Pi/Qi)/log_2$, where Pi is the probability of an eCLIP-seq read at that position and Qi is the probability of input reads at that position. Results were filtered using cutoffs of 3 for both log_{10} p-values and log_2 fold changes to define a set of true peaks normalized above their respective size-matched input background signal.

For ADAR RIP experiments, Th17 cells were lysed in 25 mM Tris pH 8.0, 100 mM NaCl, 0.5% NP40, 10 mM MgCl2, 10% glycerol with RNase and protease inhibitors for 30 min on ice. Samples were spun down at 14,000 x g for 15 min, and soluble protein lysates were harvested and immunoprecipitated with control or anti-ADAR2 specific antibody as listed on Table S5.

Protein and Western Blot Analysis

For whole cell lysates, cells were lysed in 25 mM Tris pH 8.0, 100 mM NaCl, 0.5% NP40 with protease inhibitors for 30 min on ice. Samples were spun down at 14,000 x *g* for 15 min, and soluble protein lysates were harvested. The NE-PER™ kit (ThermoFisher Scientific) was used for cytoplasmic and nuclear fractionation studies. 30-50 µg protein

were loaded on each lane. Blots were blocked in Odyssey Blocking buffer (Li-CoR Biosciences) and probed with primary antibodies (Table S5). Following incubation with respective IRDye secondary antibody (Li-CoR Biosciences), infrared signals on each blot were measured on the Li-CoR Odyssey CLX.

cDNA Synthesis, qRT-PCR, and RT-PCR Sanger Analysis

Total RNA was extracted with the RNeasy kit (QIAGEN) and reverse transcribed using iScript™ Select cDNA Synthesis Kit (Bio-Rad Laboratories). Real time RT-PCR was performed using iTaq™ Universal SYBR® Green Supermix (Bio-Rad Laboratories). Expression data was normalized to Gapdh mRNA levels. qRT-PCR primers were designed using Primer-BLAST to span across splice junctions, resulting in PCR amplicons that span at least one intron. Primer sequences are listed in Table S4.

To assess the fraction of candidate transcripts carrying A-to-I edits, RT-PCR was performed on Th17 cDNAs using the Q5 Hot Start High-Fidelity 2X Master Mix (New England Biolabs) with the standard thermocycling protocol. Samples were incubated at 98 ˚C for 30 seconds, followed by a denaturation for 10 s at 98 ˚C, 20 s at 66 ˚C, and 72 ˚C for 1 min for a total of 34 cycles. PCR products were purified using Quick PCR Purification Kit (Qiagen) and sequenced. Primers are listed in Table S4.

Statistical Analysis

All values are presented as means ± SD. Significant differences were evaluated using GraphPad Prism 8 software. The Student's t-test or paired t-test were used to determine

significant differences between two groups. A two-tailed p-value of <0.05 was considered statistically significant in all experiments.

SUPPLEMENTAL INFORMATION

Figure S1. **Expression of genes encoding ADARs in different T helper subsets**

A. RNA expression of *Adar*, *Adarb1*, and *Adarb2* in naive and different polarized T helper subsets (Stubbington et al., 2015).

Figure S2. **ADAR2 nuclear localization in Th17 cells**

A. Representative western blot analysis of cytoplasmic and nuclear extracts from WT Th17 cells. This experiment was repeated two times on independent biological samples with similar results.

Figure S3. **Chromatin accessibility of putative Adarb1 enhancers correlates with promoter openness**

A. Normalized ATAC-seq read count at the *Adarb1* promoter and putative cis-regulatory elements in the 0 (naive), 48, or 72-hour time points were used to calculate co-openness correlation scores.

Figure S4. **ADAR2 associates with *Hif1a* transcripts in Th17 cells**

A. Wildtype Th17 cells polarized in culture for 72 hours were lysed and immunoprecipitated with control or ADAR2 specific antibodies. Hif1a pre-mRNA or mature mRNA in input and immunoprecipitated samples were quantified by qRT-

PCR. Average and standard deviation from two biological replicates are shown. * *p*-value<0.05.

Figure S5. **Splicing assessment of the *Hif1a* and *Adarb1* transcripts**

A. Primers designed to amplify *Hif1a* transcript (exon 11-intro 11 and exon 11-exon 12 junction) and *Adrb1* transcript (exon 4-intron 4 and exon 4-exon 5 junction) by RT-PCR. Splicing frequency was calculated as the ratio of unspliced RNA over spliced mRNA in each condition.

Figure S6. **Abundant RNA and protein expression of DDX5 in Th17 cells**

A. RNA expression of transcripts encoding various RBPs in $CD4^+$ naive and different polarized T helper subsets (Stubbington et al., 2015).
B. Western blot analysis confirmed efficient immunoprecipitation of DDX5 from two independent replicates of Th17 cell lysates.

Figure S7. **Expression of select DDX5 dependent and independent genes in Th17 cells**

A. DEseq2 quantified RNA expression of *Batf, Irf4,* and *Rorc* in Th17 cells from WT^T (n=2) and $DDX5^{\Delta T}$ (n=2) mice. Each dot represents result from one biological replicate.
B. DEseq2 quantified RNA expression of *Adar* and *Adarb1* in Th17 cells from WT^T (n=2) and $DDX5^{\Delta T}$ (n=2) mice. Each dot represents result from one biological replicate. * *p*-value<0.05, **** *p*-value<0.001.

Figure S8. **Identification and validation of DDX5-dependent A-to-I editing in Th17 cells**

A. Scatterplot of SAILOR analysis on two independent biological replicates of Th17 cells from WT^{T} and $DDX5^{\Delta T}$ mice.
B. Results from SAILOR analysis on *Hif1a* and *Apobec3* transcripts in two pairs of WT^{T} and $DDX5^{\Delta T}$ Th17 cells.
C. Representative RT-PCR and Sanger sequencing analyses of the *Apobec3* RNAs from two additional pairs of WT^{T} and $DDX5^{\Delta T}$ Th17 samples independent from B.

Table S1. **SAILOR analysis of $CD4^{+}$ naive and Th17 cells**

Table S2. **SAILOR analysis of Th17 cells from WT^{T} and $DDX5^{\Delta T}$ mice**

Table S3. **sgRNA information**

Table S4. **Primer information**

Table S5. **Antibody information**

REFERENCES

Anantharaman, A., Tripathi, V., Khan, A., Yoon, J.H., Singh, D.K., Gholamalamdari, O., Guang, S., Ohlson, J., Wahlstedt, H., Ohman, M.*, et al.* (2017). ADAR2 regulates RNA stability by modifying access of decay-promoting RNA-binding proteins. Nucleic Acids Res *45*, 4189-4201.

Aschenbrenner, D., Foglierini, M., Jarrossay, D., Hu, D., Weiner, H.L., Kuchroo, V.K., Lanzavecchia, A., Notarbartolo, S., and Sallusto, F. (2018). An immunoregulatory and tissue-residency program modulated by c-MAF in human TH17 cells. Nat Immunol *19*, 1126-1136.

Athanasiadis, A., Rich, A., and Maas, S. (2004). Widespread A-to-I RNA editing of Alu-containing mRNAs in the human transcriptome. PLoS Biol *2*, e391.

Bellemore, S.M., Nikoopour, E., Schwartz, J.A., Krougly, O., Lee-Chan, E., and Singh, B. (2015). Preventative role of interleukin-17 producing regulatory T helper type 17 (Treg 17) cells in type 1 diabetes in non-obese diabetic mice. Clin Exp Immunol *182*, 261-269.

Buenrostro, J.D., Wu, B., Chang, H.Y., and Greenleaf, W.J. (2015). ATAC-seq: A Method for Assaying Chromatin Accessibility Genome-Wide. Curr Protoc Mol Biol *109*, 21 29 21-21 29 29.

Chalk, A.M., Taylor, S., Heraud-Farlow, J.E., and Walkley, C.R. (2019). The majority of A-to-I RNA editing is not required for mammalian homeostasis. Genome Biol *20*, 268.

Chaudhry, A., Samstein, R.M., Treuting, P., Liang, Y., Pils, M.C., Heinrich, J.M., Jack, R.S., Wunderlich, F.T., Bruning, J.C., Muller, W.*, et al.* (2011). Interleukin-10 signaling in regulatory T cells is required for suppression of Th17 cell-mediated inflammation. Immunity *34*, 566-578.

Ciofani, M., Madar, A., Galan, C., Sellars, M., Mace, K., Pauli, F., Agarwal, A., Huang, W., Parkhurst, C.N., Muratet, M.*, et al.* (2012). A validated regulatory network for Th17 cell specification. Cell *151*, 289-303.

Codarri, L., Gyulveszi, G., Tosevski, V., Hesske, L., Fontana, A., Magnenat, L., Suter, T., and Becher, B. (2011). RORgammat drives production of the cytokine GM-CSF in helper T cells, which is essential for the effector phase of autoimmune neuroinflammation. Nat Immunol *12*, 560-567.

Dang, E.V., Barbi, J., Yang, H.Y., Jinasena, D., Yu, H., Zheng, Y., Bordman, Z., Fu, J., Kim, Y., Yen, H.R.*, et al.* (2011). Control of T(H)17/T(reg) balance by hypoxia-inducible factor 1. Cell *146*, 772-784.

Dobin, A., Davis, C.A., Schlesinger, F., Drenkow, J., Zaleski, C., Jha, S., Batut, P., Chaisson, M., and Gingeras, T.R. (2013). STAR: ultrafast universal RNA-seq aligner. Bioinformatics *29*, 15-21.

Esplugues, E., Huber, S., Gagliani, N., Hauser, A.E., Town, T., Wan, Y.Y., O'Connor, W., Jr., Rongvaux, A., Van Rooijen, N., Haberman, A.M.*, et al.* (2011). Control of TH17 cells occurs in the small intestine. Nature *475*, 514-518.

Gallo, A., Vukic, D., Michalik, D., O'Connell, M.A., and Keegan, L.P. (2017). ADAR RNA editing in human disease; more to it than meets the I. Hum Genet *136*, 1265-1278.

Higuchi, M., Maas, S., Single, F.N., Hartner, J., Rozov, A., Burnashev, N., Feldmeyer, D., Sprengel, R., and Seeburg, P.H. (2000). Point mutation in an AMPA receptor gene rescues lethality in mice deficient in the RNA-editing enzyme ADAR2. Nature *406*, 78-81.

Hueber, W., Sands, B.E., Lewitzky, S., Vandemeulebroecke, M., Reinisch, W., Higgins, P.D., Wehkamp, J., Feagan, B.G., Yao, M.D., Karczewski, M.*, et al.* (2012). Secukinumab,

a human anti-IL-17A monoclonal antibody, for moderate to severe Crohn's disease: unexpected results of a randomised, double-blind placebo-controlled trial. Gut *61*, 1693-1700.

Kaikkonen, M.U., Spann, N.J., Heinz, S., Romanoski, C.E., Allison, K.A., Stender, J.D., Chun, H.B., Tough, D.F., Prinjha, R.K., Benner, C.*, et al.* (2013). Remodeling of the enhancer landscape during macrophage activation is coupled to enhancer transcription. Mol Cell *51*, 310-325.

Labun, K., Montague, T.G., Krause, M., Torres Cleuren, Y.N., Tjeldnes, H., and Valen, E. (2019). CHOPCHOP v3: expanding the CRISPR web toolbox beyond genome editing. Nucleic Acids Res *47*, W171-W174.

Landt, S.G., Marinov, G.K., Kundaje, A., Kheradpour, P., Pauli, F., Batzoglou, S., Bernstein, B.E., Bickel, P., Brown, J.B., Cayting, P.*, et al.* (2012). ChIP-seq guidelines and practices of the ENCODE and modENCODE consortia. Genome Res *22*, 1813-1831.

Li, H., Handsaker, B., Wysoker, A., Fennell, T., Ruan, J., Homer, N., Marth, G., Abecasis, G., Durbin, R., and Genome Project Data Processing, S. (2009). The Sequence Alignment/Map format and SAMtools. Bioinformatics *25*, 2078-2079.

Liao, Y., Smyth, G.K., and Shi, W. (2014). featureCounts: an efficient general purpose program for assigning sequence reads to genomic features. Bioinformatics *30*, 923-930.

Lin, C., Yang, L., Yang, J.J., Huang, Y., and Liu, Z.R. (2005). ATPase/helicase activities of p68 RNA helicase are required for pre-mRNA splicing but not for assembly of the spliceosome. Mol Cell Biol *25*, 7484-7493.

Liu, Z.R. (2002). p68 RNA helicase is an essential human splicing factor that acts at the U1 snRNA-5' splice site duplex. Mol Cell Biol *22*, 5443-5450.

Love, M.I., Huber, W., and Anders, S. (2014). Moderated estimation of fold change and dispersion for RNA-seq data with DESeq2. Genome Biol *15*, 550.

Loven, J., Hoke, H.A., Lin, C.Y., Lau, A., Orlando, D.A., Vakoc, C.R., Bradner, J.E., Lee, T.I., and Young, R.A. (2013). Selective inhibition of tumor oncogenes by disruption of super-enhancers. Cell *153*, 320-334.

McGeachy, M.J., Bak-Jensen, K.S., Chen, Y., Tato, C.M., Blumenschein, W., McClanahan, T., and Cua, D.J. (2007). TGF-beta and IL-6 drive the production of IL-17 and IL-10 by T cells and restrain T(H)-17 cell-mediated pathology. Nat Immunol *8*, 1390-1397.

Meng, X., Grotsch, B., Luo, Y., Knaup, K.X., Wiesener, M.S., Chen, X.X., Jantsch, J., Fillatreau, S., Schett, G., and Bozec, A. (2018). Hypoxia-inducible factor-1alpha is a critical transcription factor for IL-10-producing B cells in autoimmune disease. Nat Commun *9*, 251.

Morita, S., Kojima, T., and Kitamura, T. (2000). Plat-E: an efficient and stable system for transient packaging of retroviruses. Gene therapy *7*, 1063-1066.

Nakahama, T., Kato, Y., Kim, J.I., Vongpipatana, T., Suzuki, Y., Walkley, C.R., and Kawahara, Y. (2018). ADAR1-mediated RNA editing is required for thymic self-tolerance and inhibition of autoimmunity. EMBO Rep *19*.

Nicol, S.M., Bray, S.E., Black, H.D., Lorimore, S.A., Wright, E.G., Lane, D.P., Meek, D.W., Coates, P.J., and Fuller-Pace, F.V. (2013). The RNA helicase p68 (DDX5) is selectively required for the induction of p53-dependent p21 expression and cell-cycle arrest after DNA damage. Oncogene *32*, 3461-3469.

Nicol, S.M., Bray, S.E., Derek Black, H., Lorimore, S.A., Wright, E.G., Lane, D.P., Meek, D.W., Coates, P.J., and Fuller-Pace, F.V. (2012). The RNA helicase p68 (DDX5) is selectively required for the induction of p53-dependent p21 expression and cell-cycle arrest after DNA damage. Oncogene.

Palladino, M.J., Keegan, L.P., O'Connell, M.A., and Reenan, R.A. (2000). dADAR, a Drosophila double-stranded RNA-specific adenosine deaminase is highly developmentally regulated and is itself a target for RNA editing. RNA *6*, 1004-1018.

Qi, L., Song, Y., Chan, T.H.M., Yang, H., Lin, C.H., Tay, D.J.T., Hong, H., Tang, S.J., Tan, K.T., Huang, X.X.*, et al.* (2017). An RNA editing/dsRNA binding-independent gene regulatory mechanism of ADARs and its clinical implication in cancer. Nucleic Acids Res *45*, 10436-10451.

Qiu, S., Li, W., Xiong, H., Liu, D., Bai, Y., Wu, K., Zhang, X., Yang, H., Ma, K., Hou, Y.*, et al.* (2016). Single-cell RNA sequencing reveals dynamic changes in A-to-I RNA editome during early human embryogenesis. BMC Genomics *17*, 766.

Ran, F.A., Hsu, P.D., Wright, J., Agarwala, V., Scott, D.A., and Zhang, F. (2013). Genome engineering using the CRISPR-Cas9 system. Nat Protoc *8*, 2281-2308.

Reiner, S.L. (2009). Decision making during the conception and career of CD4+ T cells. Nat Rev Immunol *9*, 81-82.

Stockinger, B., and Omenetti, S. (2017). The dichotomous nature of T helper 17 cells. Nat Rev Immunol *17*, 535-544.

Stubbington, M.J., Mahata, B., Svensson, V., Deonarine, A., Nissen, J.K., Betz, A.G., and Teichmann, S.A. (2015). An atlas of mouse CD4(+) T cell transcriptomes. Biol Direct *10*, 14.

Tan, M.H., Li, Q., Shanmugam, R., Piskol, R., Kohler, J., Young, A.N., Liu, K.I., Zhang, R., Ramaswami, G., Ariyoshi, K.*, et al.* (2017). Dynamic landscape and regulation of RNA editing in mammals. Nature *550*, 249-254.

Tanaka, S., Jiang, Y., Martinez, G.J., Tanaka, K., Yan, X., Kurosaki, T., Kaartinen, V., Feng, X.H., Tian, Q., Wang, X.*, et al.* (2018). Trim33 mediates the proinflammatory function of Th17 cells. J Exp Med *215*, 1853-1868.

Tang, S.J., Shen, H., An, O., Hong, H., Li, J., Song, Y., Han, J., Tay, D.J.T., Ng, V.H.E., Bellido Molias, F.*, et al.* (2020). Cis- and trans-regulations of pre-mRNA splicing by RNA editing enzymes influence cancer development. Nat Commun *11*, 799.

Thorvaldsdottir, H., Robinson, J.T., and Mesirov, J.P. (2013). Integrative Genomics Viewer (IGV): high-performance genomics data visualization and exploration. Brief Bioinform *14*, 178-192.

Tigno-Aranjuez, J.T., Jaini, R., Tuohy, V.K., Lehmann, P.V., and Tary-Lehmann, M. (2009). Encephalitogenicity of complete Freund's adjuvant relative to CpG is linked to induction of Th17 cells. J Immunol *183*, 5654-5661.

Van Nostrand, E.L., Pratt, G.A., Shishkin, A.A., Gelboin-Burkhart, C., Fang, M.Y., Sundararaman, B., Blue, S.M., Nguyen, T.B., Surka, C., Elkins, K.*, et al.* (2016). Robust transcriptome-wide discovery of RNA-binding protein binding sites with enhanced CLIP (eCLIP). Nat Methods *13*, 508-514.

Volchenkov, R., Nygaard, V., Sener, Z., and Skalhegg, B.S. (2017). Th17 Polarization under Hypoxia Results in Increased IL-10 Production in a Pathogen-Independent Manner. Front Immunol *8*, 698.

Walkley, C.R., and Li, J.B. (2017). Rewriting the transcriptome: adenosine-to-inosine RNA editing by ADARs. Genome Biol *18*, 205.

Washburn, M.C., Kakaradov, B., Sundararaman, B., Wheeler, E., Hoon, S., Yeo, G.W., and Hundley, H.A. (2014). The dsRBP and inactive editor ADR-1 utilizes dsRNA binding to regulate A-to-I RNA editing across the C. elegans transcriptome. Cell Rep *6*, 599-607.

Wu, X., Tian, J., and Wang, S. (2018). Insight Into Non-Pathogenic Th17 Cells in Autoimmune Diseases. Front Immunol *9*, 1112.

Yasuda, K., Takeuchi, Y., and Hirota, K. (2019). The pathogenicity of Th17 cells in autoimmune diseases. Semin Immunopathol *41*, 283-297.

Zhang, Y., Liu, T., Meyer, C.A., Eeckhoute, J., Johnson, D.S., Bernstein, B.E., Nusbaum, C., Myers, R.M., Brown, M., Li, W.*, et al.* (2008). Model-based analysis of ChIP-Seq (MACS). Genome Biol *9*, R137.

Zhou, B., Li, X., Luo, D., Lim, D.H., Zhou, Y., and Fu, X.D. (2019). GRID-seq for comprehensive analysis of global RNA-chromatin interactions. Nat Protoc *14*, 2036-2068.

Figure 1. **An intragenic super enhancer promotes *Adarb1* transcription in Th17 cells**

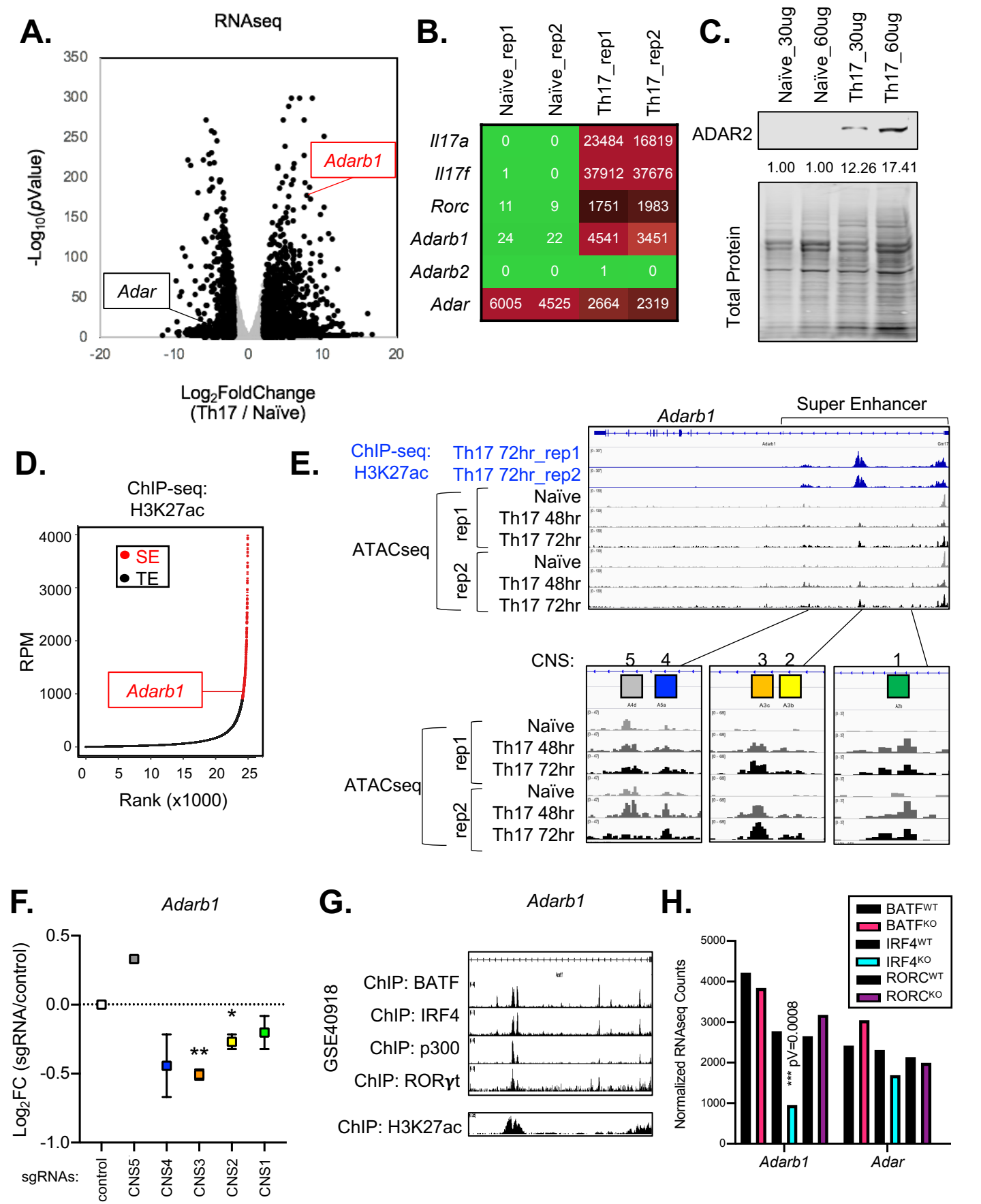

Figure 2. **Overlapping and unique A-to-I editomes in wild type naive and Th17 cells**

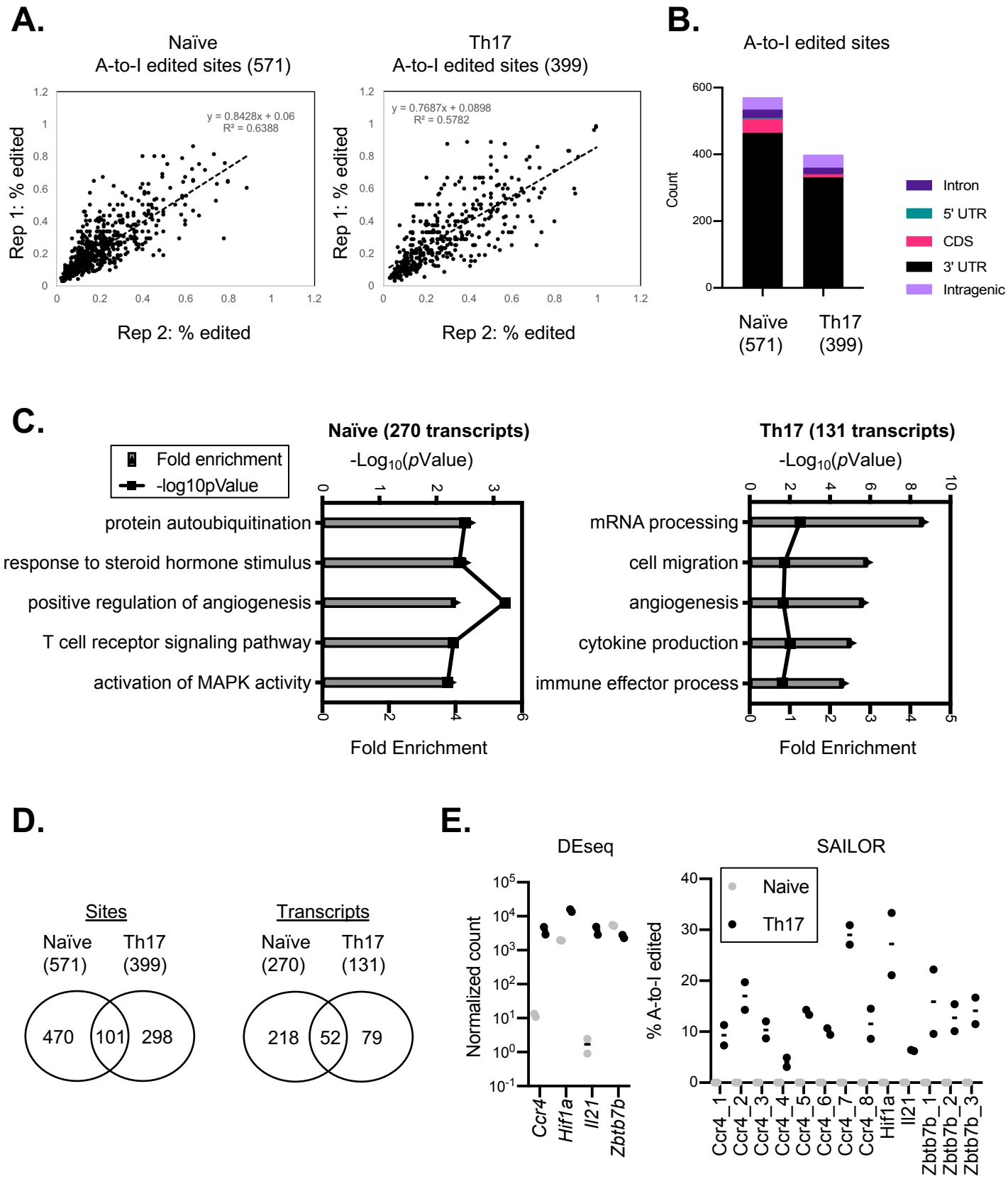

Figure 3. **ADAR2 negatively regulates HIF1α expression in Th17 cells**

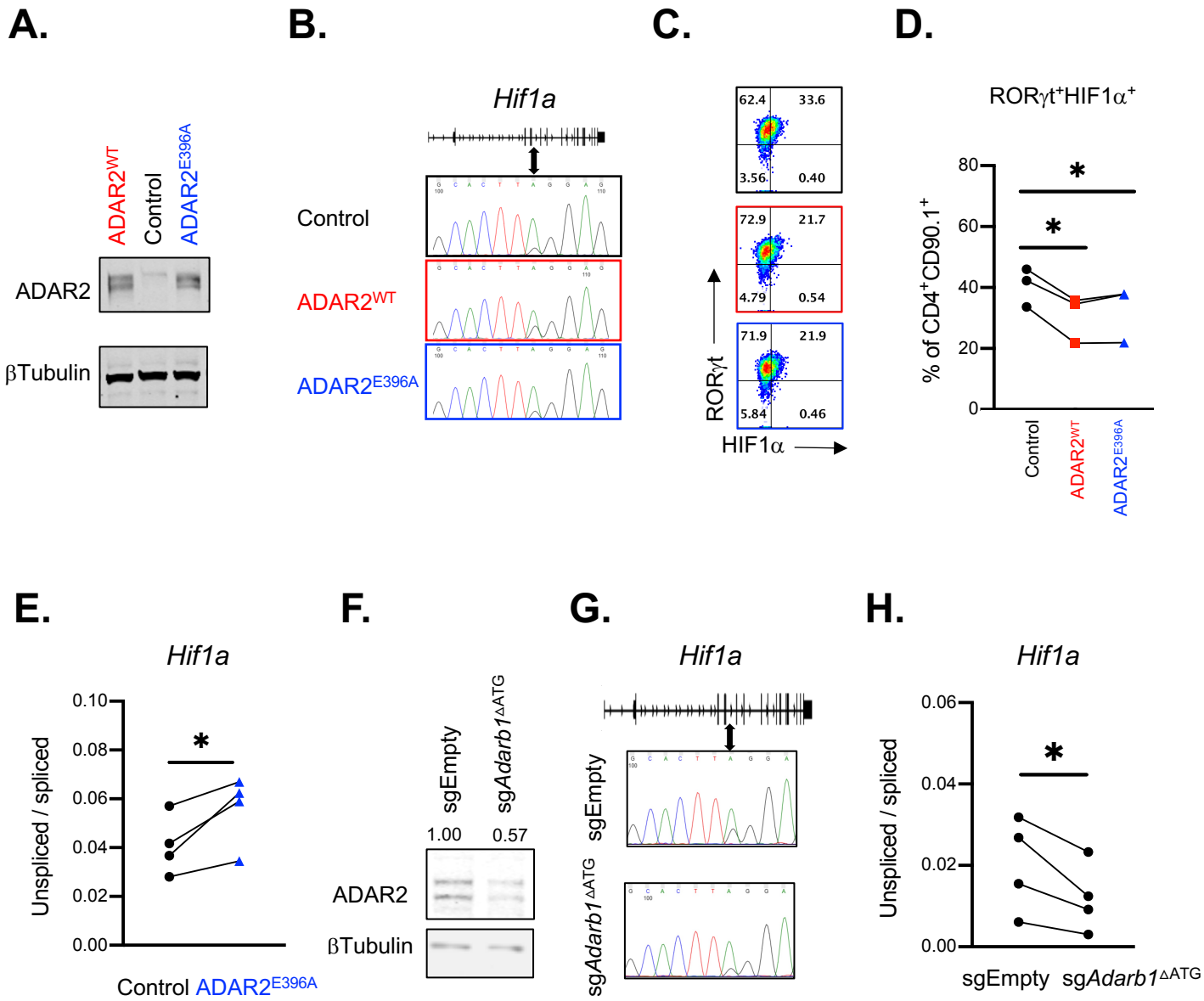

Figure 4. **ADAR2-HIF1α regulates IL-10 production in Th17 cells *in vitro* and *in vivo***

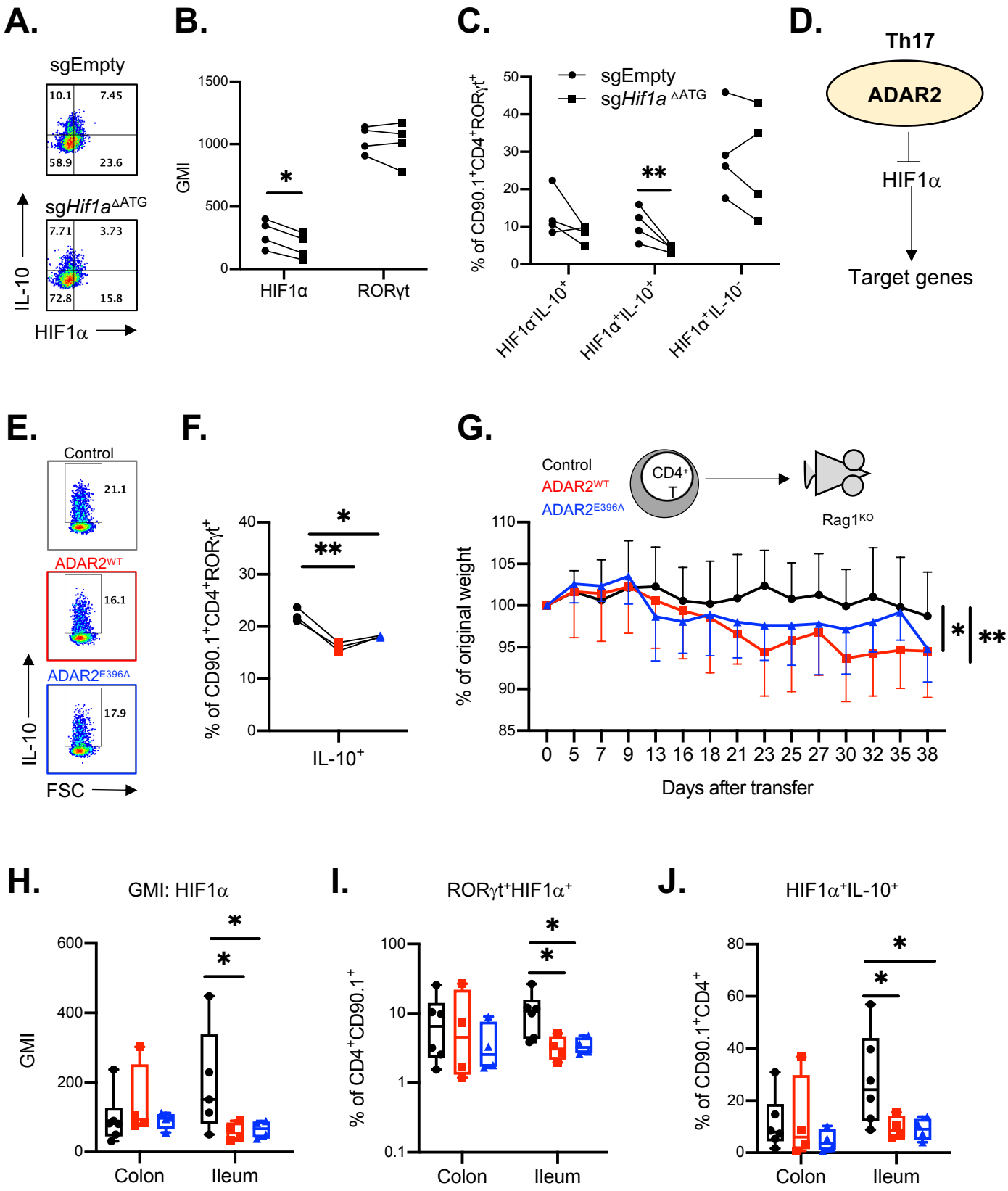

Figure 5. ***Adarb1* is post-transcriptionally regulated by RNA binding protein DDX5**

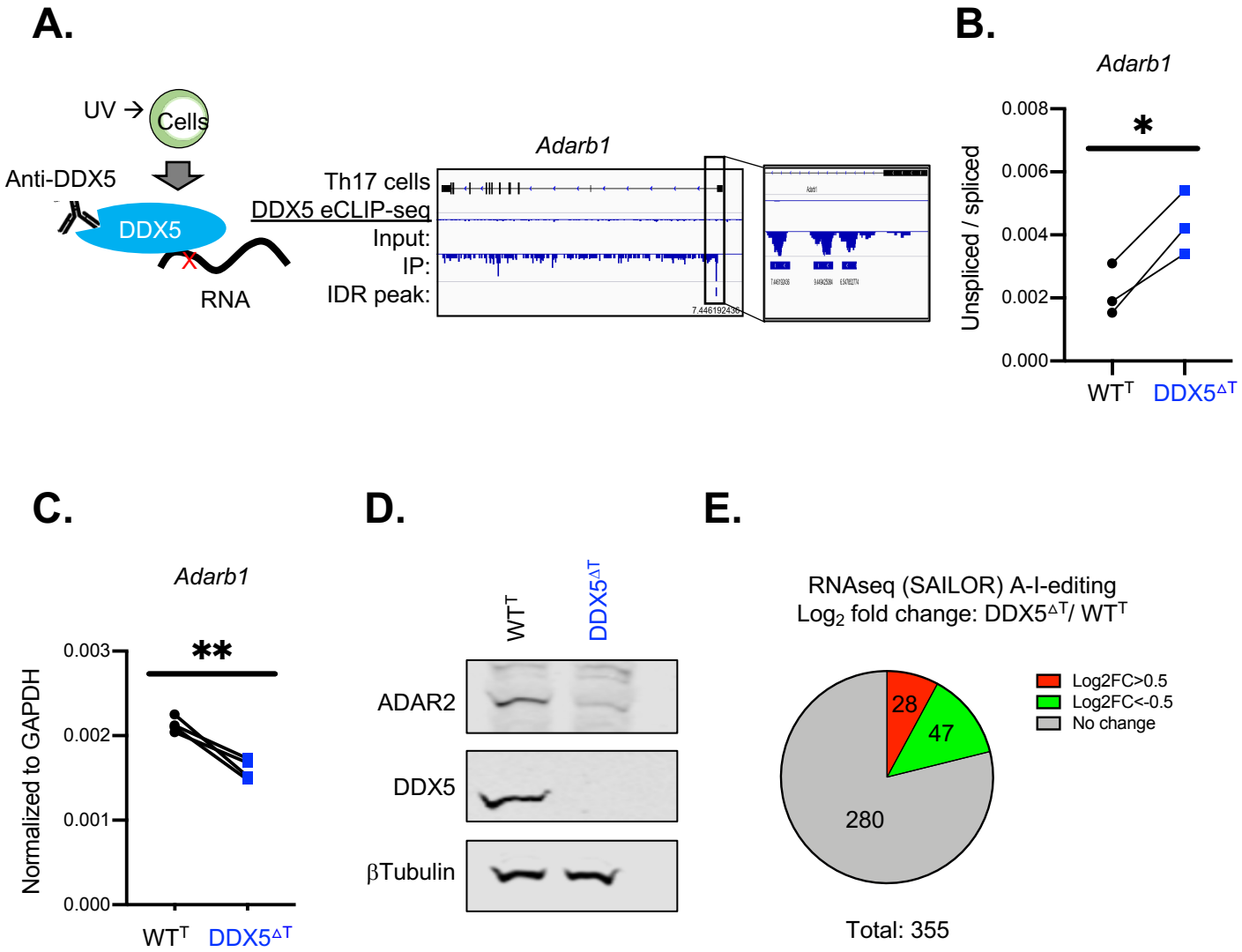

Figure 6. **DDX5 promotes HIF1a-IL-10 axis *in vitro* and *in vivo***

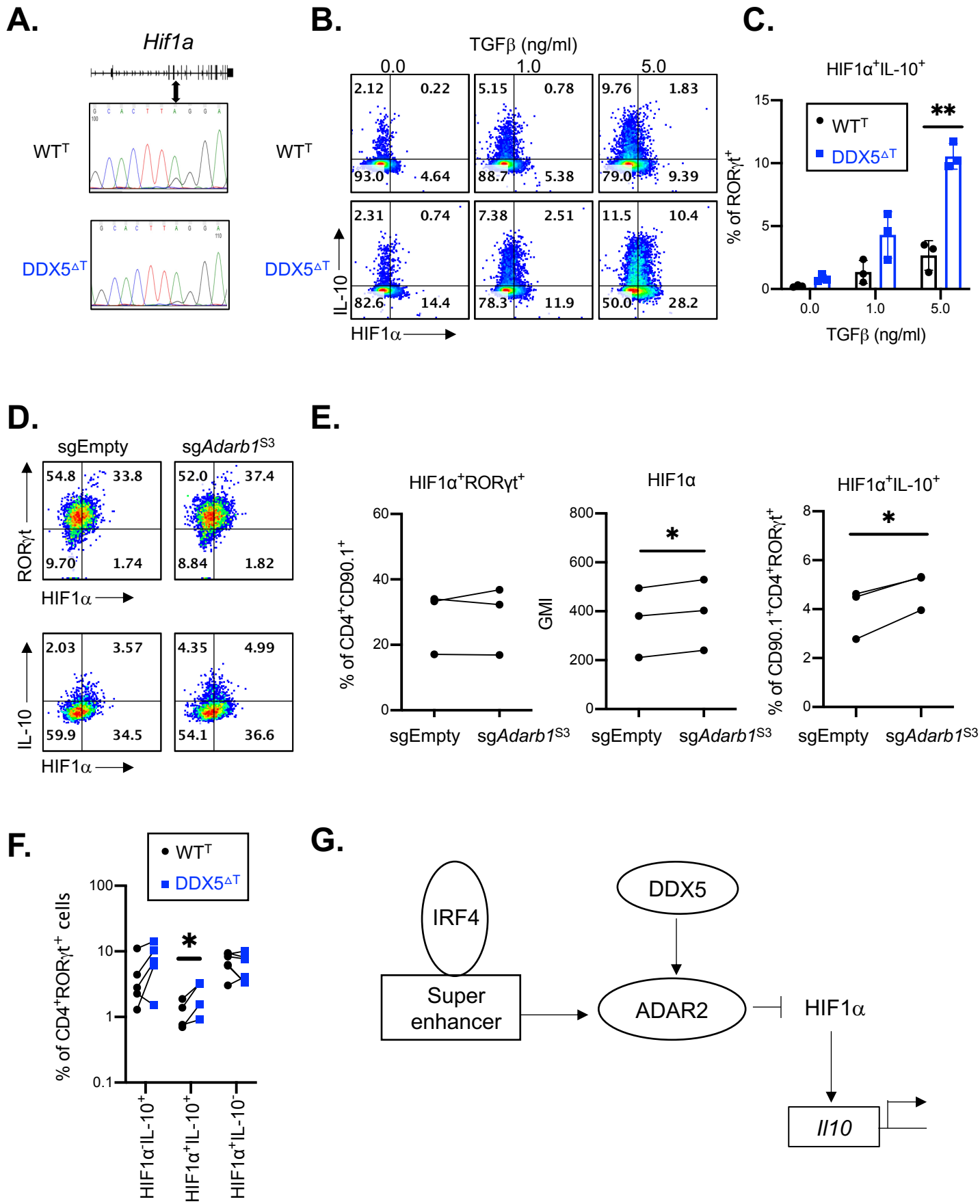

Supplementary Figures

Figure S1. **ADARs gene expression in different T helper subsets**

A.

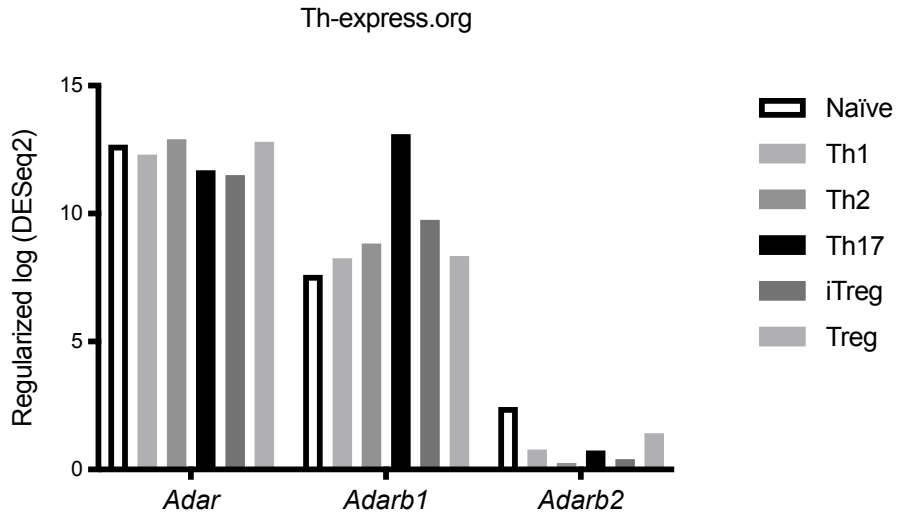

Figure S2. **ADAR2 nuclear localization in Th17 cells**

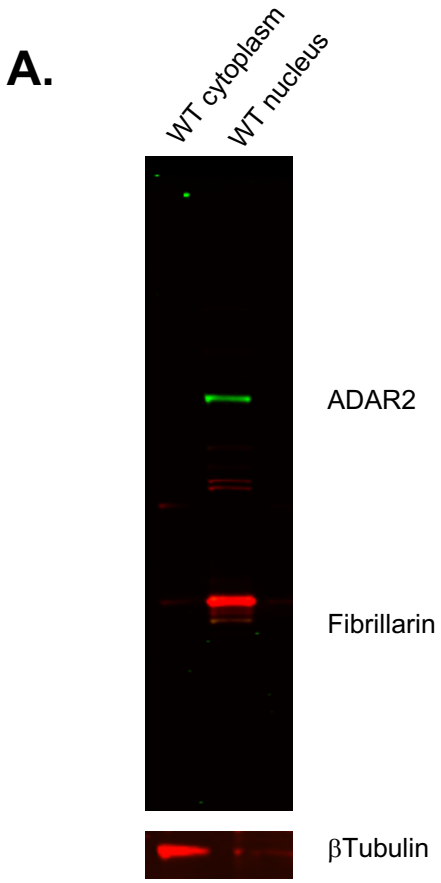

Figure S3. **Chromatin accessibility of putative *Adarb1* enhancers correlates with promoter openness**

A.

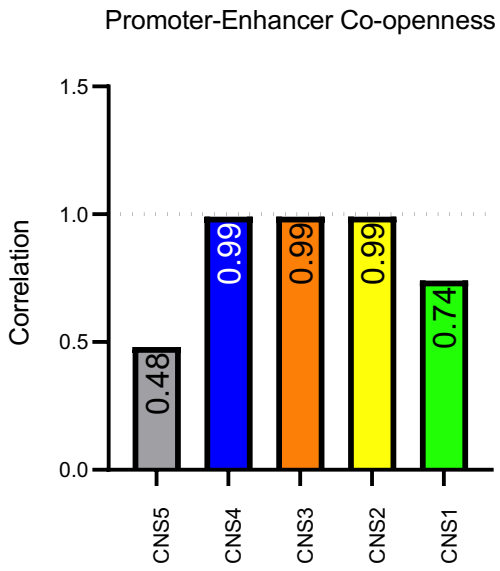

Figure S4. ***Hif1a* transcript associates with ADAR2 in Th17 cells**

A.

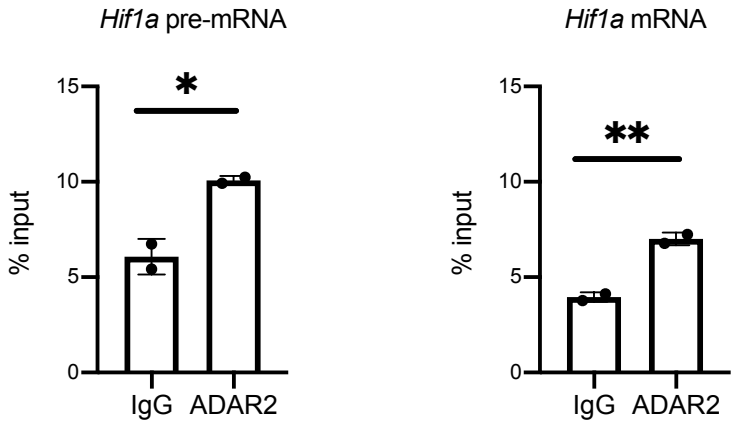

Figure S5. **Splicing assessment of the *Hif1a* and *Adarb1* transcripts**

A.

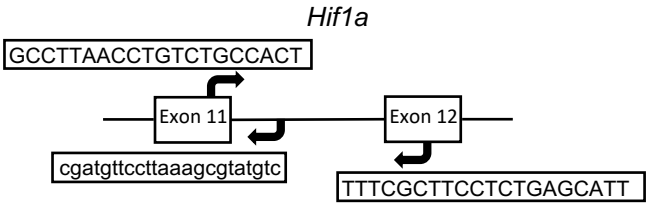

$$\frac{Hif1a\ unspliced\ mRNA}{Hif1a\ spliced\ mRNA} = \textit{Hif1a}\ \text{splicing ratio}$$

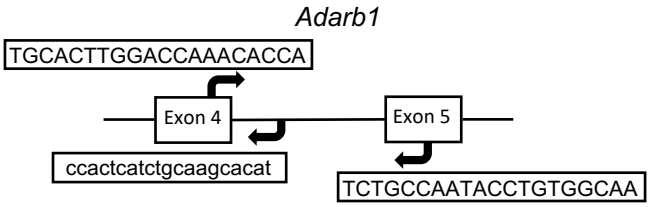

$$\frac{Adarb1\ unspliced\ mRNA}{Adarb1\ spliced\ mRNA} = \textit{Adarb1}\ \text{splicing ratio}$$

Figure S6. **Abundant RNA and protein expression of DDX5 in Th17 cells**

A.

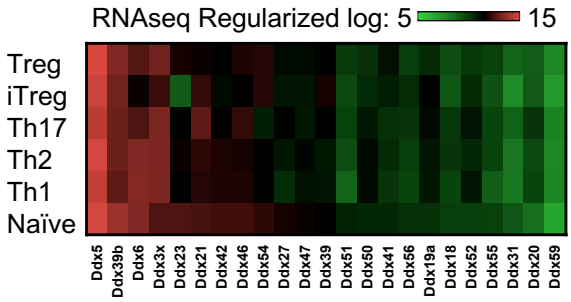

B.

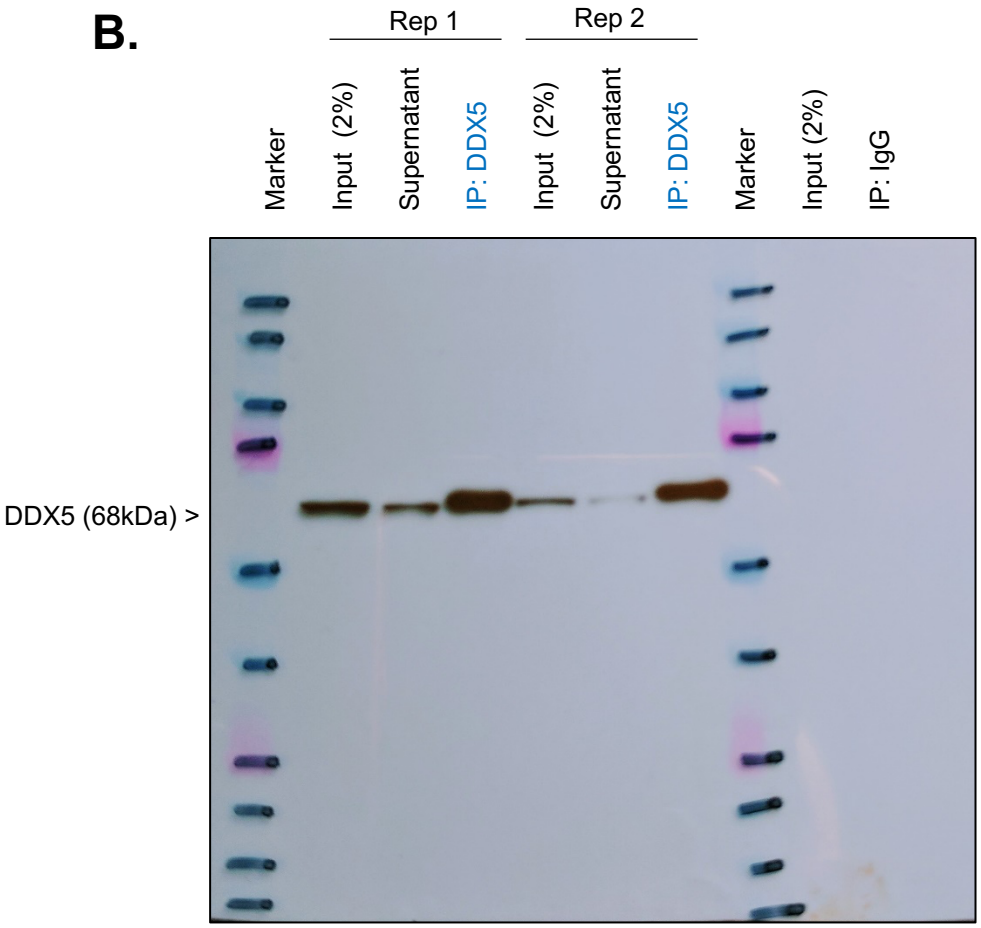

Figure S7. **Expression of select DDX5 dependent and independent genes in Th17 cells**

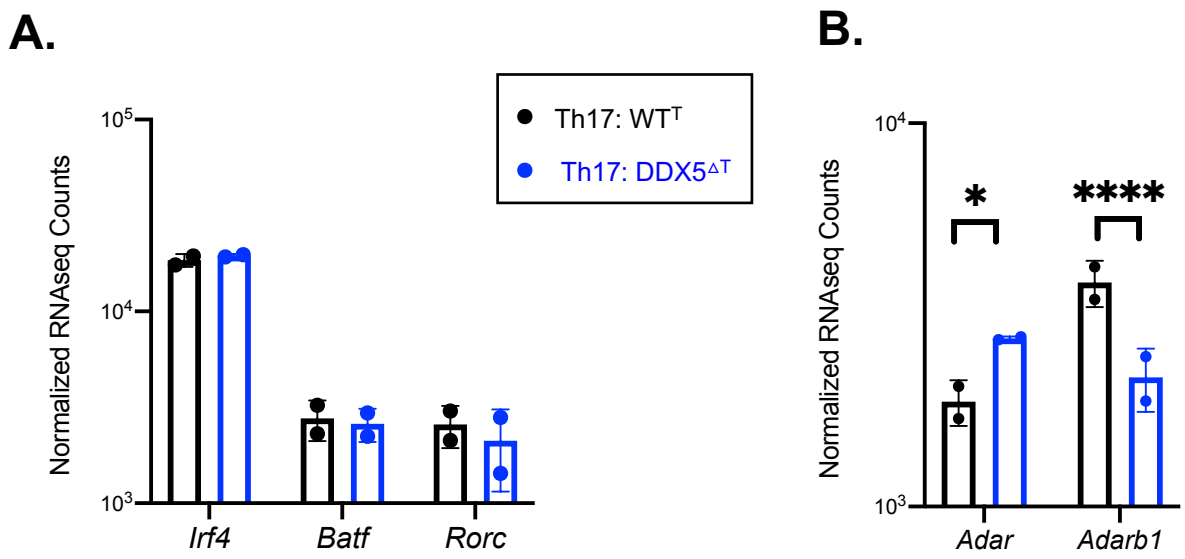

Figure S8. **Identification and validation of DDX5-dependent A-to-I editing in Th17 cells**

A.

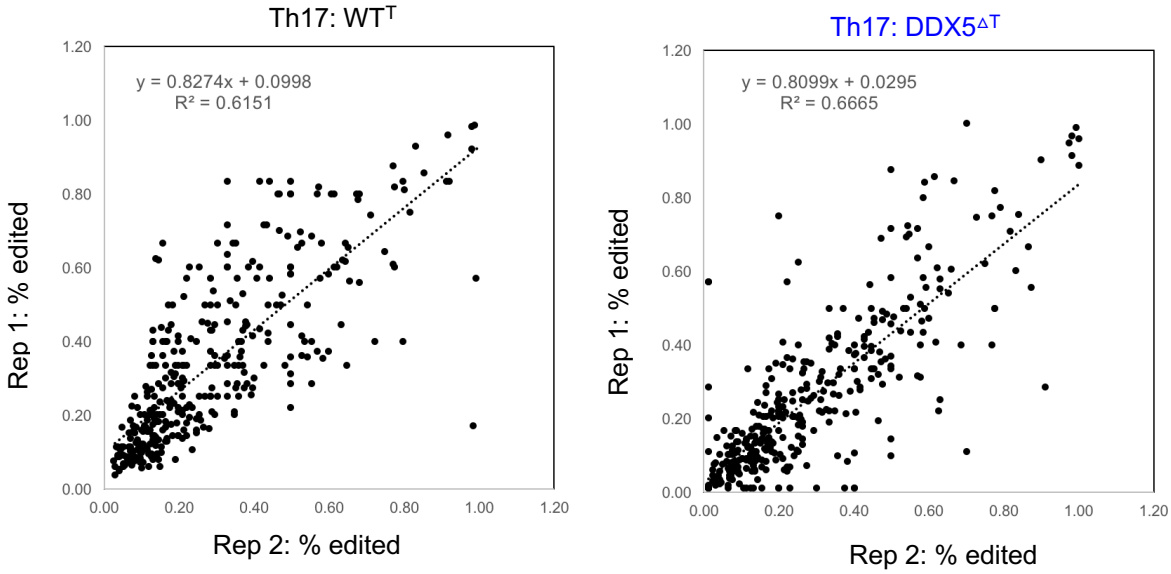

B.

Hif1a

RNAseq	A-to-I Editing
WT^{T} rep1	20.0
DDX5$^{\Delta T}$_rep1	7.0
WT^{T} rep2	29.8
DDX5$^{\Delta T}$_rep2	2.6

Apobec3

RNAseq	A-to-I Editing
WT^{T} rep1	15.6
DDX5$^{\Delta T}$_rep1	7.3
WT^{T} rep2	11.4
DDX5$^{\Delta T}$_rep2	4.4

C.

Apobec3

Sanger	A-to-I Editing
WT^{T} rep3	16.8
DDX5$^{\Delta T}$_rep3	7.1
WT^{T} rep4	22.9
DDX5$^{\Delta T}$_rep4	9.3

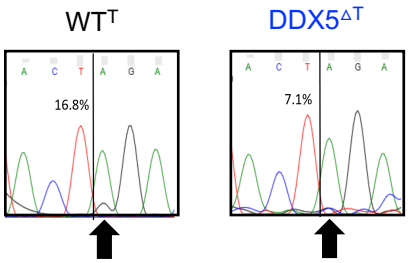

Graphic Abstract

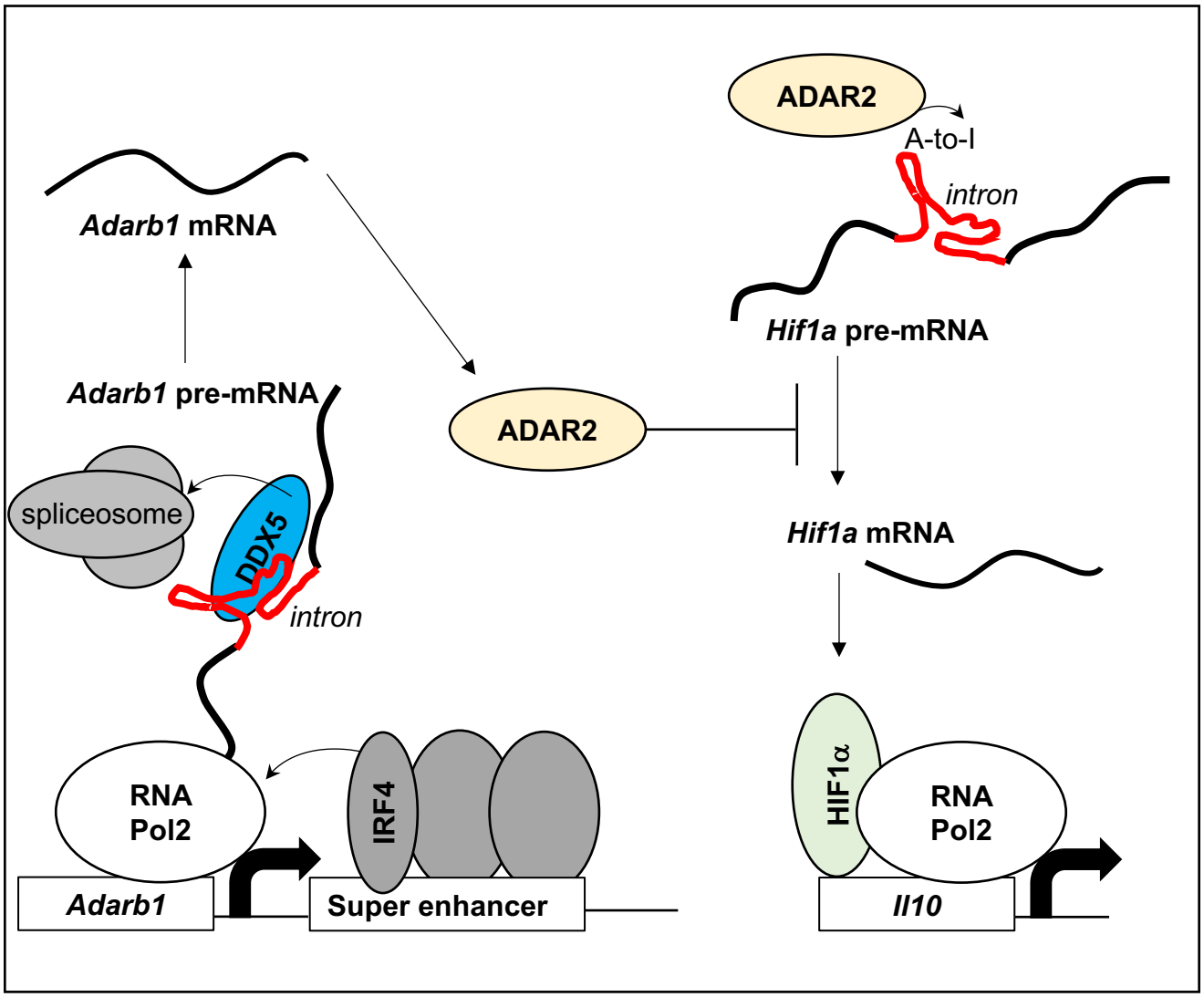

Major findings:

Naïve and Th17 cells harbored overlapping and unique A-to-I editome.

ADAR2 expression is induced during Th17 polarization under the control of an intragenic super enhancer.

ADAR2 targets *Hif1a* transcripts to regulate HIF1α expression and IL-10 production in RORγt$^+$ Th17 cells in the small intestine.

Post-transcriptionally, *Adarb1* pre-mRNAs are bound and regulated by RNA binding DEAD-box protein DDX5. DDX5-deficient Th17 cells have a dysregulated RNA editome and altered effector function.